PHYSICAL REVIEW B **82**, 085413 (2010)

# Controlling water dissociation on an ultrathin MgO film by tuning film thickness

Jaehoon Jung,[1,2] Hyung-Joon Shin,[2,3] Yousoo Kim,[2,*,†] and Maki Kawai[1,3,*,‡]
[1]*Department of Advanced Materials Science, The University of Tokyo, 5-1-5 Kashiwanoha, Kashiwa, Chiba 277-8561, Japan*
[2]*RIKEN Advanced Science Insititute, 2-1 Hirosawa, Wako, Saitama 351-0198, Japan*
[3]*Department of Applied Chemistry, The University of Tokyo, 7-3-1 Hongo, Bunkyo-ku, Tokyo 113-8656, Japan*
(Received 9 April 2010; revised manuscript received 11 June 2010; published 10 August 2010)

Periodic density-functional theory calculations at the single-molecule level were used to study dissociation of water on ultrathin MgO films with varying thickness deposited on the Ag(100) surface. The enhanced chemical activity for water dissociation on MgO/Ag(100) originates from the greater stability of dissociated products, which is due in turn to the strong hybridization of their electronic states at the oxide-metal interface. Our results provide insights into the superiority of the monolayer MgO film surface over the bulk surface and the use of the film thickness to control heterogeneous catalysis in water dissociation.

DOI: 10.1103/PhysRevB.82.085413 PACS number(s): 68.43.Bc, 68.47.Gh, 82.65.+r

The interaction of water with oxide surfaces has long been of fundamental importance to various fields of science, including geochemistry, electrochemistry, and catalysis.[1,2] Understanding how water molecules dissociate on oxide surfaces is crucial not only for revealing various solid-liquid interface phenomena but also for controlling chemical reactions involving water dissociation. Water dissociation on the MgO(100) bulk surface has so far been observed to occur only if the dissociation products are stabilized by defects or neighboring water molecules.[3–6] Compared with the MgO bulk surface, the chemical activity of water dissociation is remarkably enhanced on a single monolayer (ML) MgO film deposited on a Ag(100) surface.[7–10] In studies using high-resolution electron energy loss spectroscopy combined with x-ray photoemission spectroscopy, Savio *et al.* reported that the dissociation probability of water at room temperature on the 1-ML MgO film surface increases by a factor of 6 compared with a multilayer film.[7,8] They suggest that this remarkable enhancement in chemical reactivity originates in the border sites of the 1-ML oxide film in contact with a metal substrate. However, a theoretical study by Ferrari *et al.* does not support the role of the metal substrate at the border of the 1-ML oxide film as an explanation for the high chemical activity of the 1-ML MgO film compared with bulk MgO.[11] In photoemission and Auger electron spectroscopy experiments, Altieri *et al.* found that both border and terrace sites enhance water dissociation compared with corresponding sites of bulk MgO.[9,10] They suggest that the metal substrate beneath the terrace sites of MgO film plays a pivotal role in water dissociation. The discrepancy between these experimental results might be due to the difficulty in precisely controlling the number of defects, the size, and the thickness of the MgO thin film at a monolayer limit.[12,13]

Although experimental studies so far have definitely demonstrated the superiority of ultrathin MgO film over bulk MgO for water dissociation, such details as the phenomenon's dependence on film thickness and the contribution of defect-free terrace sites as venues for chemical activity have not been clarified and demand systematic study.[7–10] In particular, Shin *et al.* have demonstrated that the tunneling electron-induced dissociation of isolated water molecules on MgO film surfaces can be controlled depending on the film thickness.[14] This indicates that film thickness, as a controllable factor, can play an important role in determining various features of oxide films, such as catalytic and dielectric properties.[15,16]

In this study, using first-principles calculations, we examine how chemical activity on an ultrathin MgO film on the Ag(100) surface can be tuned by controlling film thickness. More specifically, we demonstrate that the enhancement of chemical activity originates from changes in geometric and electronic structures at the oxide-metal interface of the MgO/Ag(100) system.

Periodic density-functional calculations were performed using the Vienna *ab initio* simulation package (VASP) code[17,18] with the Perdew-Wang exchange-correlation functional (PW91).[19,20] The core electrons were replaced by projector-augmented wave[21] pseudopotentials, expanded in a basis set of plane waves up to a cutoff energy of 400 eV. In order to focus on the isolated single molecule without intermolecular interaction among neighboring adsorbates on the surfaces, we used $(2\sqrt{2}\times 2\sqrt{2})R45°$ surface supercells corresponding to 1/8 ML coverage of water molecules on the MgO($n$ ML)/Ag(100) ($n$=1, 2, and 3) and MgO(100) surfaces. The calculated lattice constants are 4.15 and 4.20 Å for Ag and MgO, respectively, which agrees with other theoretical and experimental values to within ~2%.[22] The slab models for the MgO($n$ ML)/Ag(100) surfaces consist of $n$ layers of MgO and four layers of Ag. The MgO(100) bulk surface was represented by a four-layer MgO slab. The periodically replicated slabs were separated by a vacuum region of ~15 Å. During ionic relaxations, two bottom Ag layers of MgO/Ag(100) and one bottom MgO layer of MgO(100) were fixed in their bulk positions. Ionic relaxations were performed until atomic forces were less than 0.01 eV/Å. $2\times 2\times 1$ and $8\times 8\times 1$ Γ-centered grids were used for the $k$-point sampling of the Brillouin zone for ionic relaxation and density of states (DOS) calculations, respectively. Electron localization function (ELF) (Ref. 23) and Bader population[24] analyses were also carried out to investigate the electronic distribution. The transition states for water dissociation were obtained using the climbing image nudged elastic band method[25] and confirmed by vibrational frequency calculations. The dipole correction was applied in order to avoid interactions between periodic slab images. All calculations were performed without any symmetry restrictions.

 

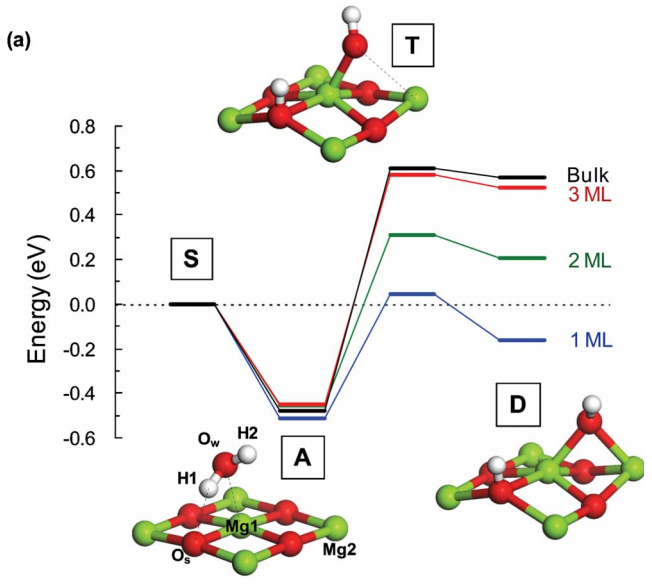


(b) (in eV)

| | *E*(A) | *E*(T) | *E*(D) | $E_a$ |
|---|---|---|---|---|
| MgO(1 ML)/Ag(100) | –0.51 | 0.05 | –0.16 | 0.56 |
| MgO(2 ML)/Ag(100) | –0.46 | 0.31 | 0.21 | 0.77 |
| MgO(3 ML)/Ag(100) | –0.45 | 0.58 | 0.53 | 1.03 |
| MgO(100) | –0.48 | 0.61 | 0.57 | 1.09 |

FIG. 1. (Color online) (a) The energy diagram (in eV) for the dissociation of a water single molecule on MgO($n$ ML)/Ag(100) ($n$=1, 2, and 3) and MgO(100) surfaces and the corresponding atomic structures for $n$=2 (H, white; O, red (grey); Mg, green (dark grey)). (b) Nondissociative adsorption (**A**), transition (**T**), and dissociative adsorption (**D**) state energies are evaluated relative to $E(H_2O)+E(\text{Substrate})=0$ eV, and the activation energy, $E_a$ is $E(\mathbf{T})-E(\mathbf{A})$.

In Fig. 1, we show the reaction energy for the dissociation of a single water molecule on a thin film of MgO($n$ ML)/Ag(100) ($n$=1, 2, and 3) and on a bulk MgO(100) surface. The diagram clearly shows that the chemical activity of the ultrathin MgO film is sensitive to film thickness. Nondissociative adsorption energies, $E(\mathbf{A})$, for the MgO film surfaces are similar to that of bulk MgO to within 0.03 eV. However, the dissociative adsorption energy, $E(\mathbf{D})$, dramatically decreases as the film thickness decreases. The dissociative adsorption of water on the 1-ML and 2-ML MgO film surfaces are more favorable than that on bulk MgO by 0.73 eV and 0.36 eV, respectively. The barrier height ($E_a$), $E(\mathbf{T})-E(\mathbf{A})$, for the 3-ML MgO film surface decreases by only 0.04 eV compared to that for the MgO bulk surface. However, the $E_a$ for water dissociation considerably decreases as the film thickness decreases; these are lower than that of the bulk MgO surface by 29% and 49% for the 2-ML and 1-ML MgO surfaces, respectively. These results clearly show that catalytic activity on ultrathin MgO films can be controlled by film thickness as indicated in the previous experimental results.[7–10,14] Furthermore, it should be noted that dissociation of an isolated water molecule on the 1-ML MgO film surface becomes thermodynamically exothermic independent of the presence of neighboring water molecules or the defects known to be prerequisites for water dissociation on the MgO(100) bulk surface.[3,4] The exothermic dissociation energy and the relatively low barrier height for water dissociation on the 1-ML MgO film surface strongly support recent experimental findings that defect-free terrace sites on an MgO film can enhance overall chemical reactivity.[10] As shown in Fig. 1, the water molecule first adsorbs asymmetrically on top of the surface magnesium, where one hydrogen atom interacts with a neighboring surface oxygen atom via hydrogen bonding. When the water molecule dissociates into $H^+ + OH^-$, $H^+$ forms a hydroxyl ion by bonding with a surface oxygen atom and $OH^-$ bonds with the two nearest-neighboring magnesium atoms. This reaction mechanism agrees well with recent computational results for the MgO(100) bulk surface.[26]

The geometric parameters of individual adsorbates for water dissociation are summarized in Table I. When a water molecule adsorbs on the MgO surface (**A**), its $O_w$-H1 distance becomes slightly longer than the O-H distance of a free water molecule due to asymmetric adsorption on the surface (see Fig. 1). The H-O-H angle also increases. For nondissociative (**A**) and dissociative (**D**) adsorption states, the geometric differences between individual adsorbates resulting from film thickness are negligible (<0.1 Å). The geometry of each adsorbate on the MgO bulk surface does not greatly differ from that on the film surface. This geometric similarity for each adsorbate implies that the remarkable change in chemical reactivity resulting from film thickness as shown in

TABLE I. The selected geometric parameters of free water molecule and adsorbates for nondissociative (**A**) and dissociative (**D**) adsorption states on MgO($n$ ML)/Ag(100) ($n$=1, 2, and 3) and MgO(100) surfaces. Distances are in angstrom and angles in degrees. The atomic notations are marked in Fig. 1.

| | | 1 ML | | 2 ML | | 3 ML | | Bulk | |
|---|---|---|---|---|---|---|---|---|---|
| | Free $H_2O$ | **A** | **D** | **A** | **D** | **A** | **D** | **A** | **D** |
| $O_w$-H1 | 0.97 | 1.02 | | 1.01 | | 1.01 | | 1.02 | |
| $O_w$-H2 | 0.97 | 0.97 | 0.97 | 0.97 | 0.97 | 0.97 | 0.97 | 0.97 | 0.97 |
| H1-$O_w$-H2 | 104.7 | 107.1 | | 106.5 | | 106.5 | | 106.4 | |
| $O_w$-Mg1 | | 2.20 | 2.06 | 2.26 | 2.07 | 2.27 | 2.08 | 2.25 | 2.10 |
| $O_w$-Mg2 | | | 2.07 | | 2.11 | | 2.13 | | 2.14 |
| H1-$O_s$ | | 1.72 | 0.98 | 1.75 | 0.98 | 1.76 | 0.98 | 1.72 | 0.98 |

TABLE II. The rumpling (in Å) of the relaxed *m*th-layer before water adsorption (**S**), at a nondissociative adsorption state (**A**), and at a dissociative adsorption state (**D**) of MgO(*n* ML)/Ag(100) (*n*=1, 2, and 3) and MgO(100) surfaces. For the MgO layer (*italic*), the rumpling is defined as maximum value, $z$(O)-$z$(Mg), where $z(M)$ is the $z$ coordinate of atom $M$. For the Ag layer, the rumpling is defined as the difference between the $z$ coordinates of the highest and lowest metal atoms in the *m*th layer.

| | 1 ML | | | 2 ML | | | 3 ML | | | Bulk | | |
|---|---|---|---|---|---|---|---|---|---|---|---|---|
| *m* | **S** | **A** | **D** | **S** | **A** | **D** | **S** | **A** | **D** | **S** | **A** | **D** |
| 1 | *0.08* | *0.37* | *0.82* | *0.04* | *0.15* | *0.75* | *0.04* | *0.15* | *0.68* | *0.05* | *0.14* | *0.60* |
| 2 | 0.00 | 0.04 | 0.07 | *0.00* | *0.04* | *0.53* | −0.01 | *0.01* | *0.27* | −0.01 | *0.03* | *0.21* |
| 3 | 0.00 | 0.02 | 0.04 | 0.00 | 0.01 | 0.08 | *0.02* | *0.02* | *0.12* | *0.00* | *0.01* | *0.04* |
| 4 | | | | 0.00 | 0.00 | 0.03 | 0.00 | 0.00 | 0.03 | | | |
| 5 | | | | | | | 0.00 | 0.00 | 0.01 | | | |

Fig. 1 does not originate in different interactions between adsorbates and the surface. Table II and Fig. 2 show the geometric change in the substrates induced by water dissociation. As shown in Table II, the extent of rumpling observed in the fully relaxed layers during the calculation indicates that strong geometric distortion at dissociative adsorption states (**D**) occurs only within the second MgO layer from the surface. Unlike MgO layers, the structures of Ag layers are not much affected by water dissociation even for the 1-ML thickness film. Moreover, in addition to the severe distortion of the first layers, the second layer of the

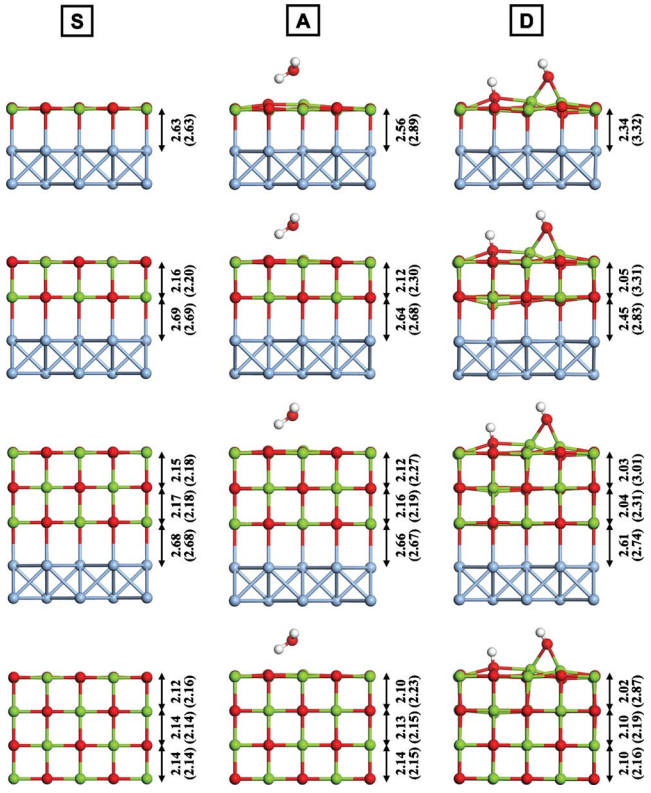


FIG. 2. (Color online) The side views of optimized structures before water adsorption (**S**), in a nondissociative adsorption state (**A**), and at a dissociative adsorption state (**D**) for the MgO(*n* ML)/Ag(100) (*n*=1, 2, and 3) and MgO(100) surfaces with the minimum (maximum) atomic distances (in Å) of the Mg-O or Ag-O bond in the $z$ direction.

2-ML MgO film also shows greater distortion than does the 3-ML MgO film or bulk MgO by about 0.3 Å. This can be attributed to a larger layer-to-layer distance at the oxide-metal interface, i.e., interface distance, which allows severe geometric distortion to accommodate the dissociation products. The minimum and maximum atomic distances between adjacent layers, $d$(Mg-O) or $d$(Ag-O), are summarized in Fig. 2. Before water adsorption (**S**), the interface distances are considerably larger than other layer-to-layer distances in MgO layers of both the films and the bulk by ~0.5 Å. It is noteworthy that the differences between minimum and maximum interface distances at dissociative adsorptive adsorption states (**D**) reach 0.98 Å and 0.38 Å for the 1-ML and 2-ML MgO films, respectively. At the oxide-metal interface, the oxygen atoms of a MgO layer are located on silver atoms and the magnesium atoms are located on the hollow site of a Ag(100) facet.[27] Geometric distortion at the oxide-metal interface includes the approach of oxygen to a silver metal atom and Mg-O bond lengthening at the Ag hollow site.

Because the geometric change during the reaction was much enhanced at the interface as well as at the surface, our study focused simultaneously on the oxide-metal interaction at the interface and the adsorbate-oxide interaction on the oxide surface. Figure 3 shows the mapping of the ELF, which reveals the electronic structures involved in those interactions. On the oxide surface, the ELF maps for dissociative adsorption products **D**($O_w$H) and **D**($O_s$H) clearly show the electrostatic interaction of $OH^-$ with a surface magnesium cation and the strong covalent bond of $H^+$ with a surface oxygen anion, respectively. While each adsorbate shows similar interactions with all the different oxide surfaces considered in this study, the pronounced polarization of the electron density under the dissociation products is found at the oxide-metal interface for the 1-ML and 2-ML MgO films [Figs. 3(a) and 3(b)]. However, in the 3-ML MgO film and in the bulk surfaces, there are no significant changes in electron density for water dissociation [Figs. 3(c) and 3(d)]. Although the covalent interaction between the MgO film and the Ag substrate is relatively weak compared to the strong ionic interaction within the MgO film, electron density polarization for the 1-ML and 2-ML MgO films [Figs. 3(a) and 3(b)] increases adhesion[28] at the interface. These results imply that enhancement of the oxide-metal interaction at the interface effectively stabilizes a dissociative adsorption state (see also Fig. 1).

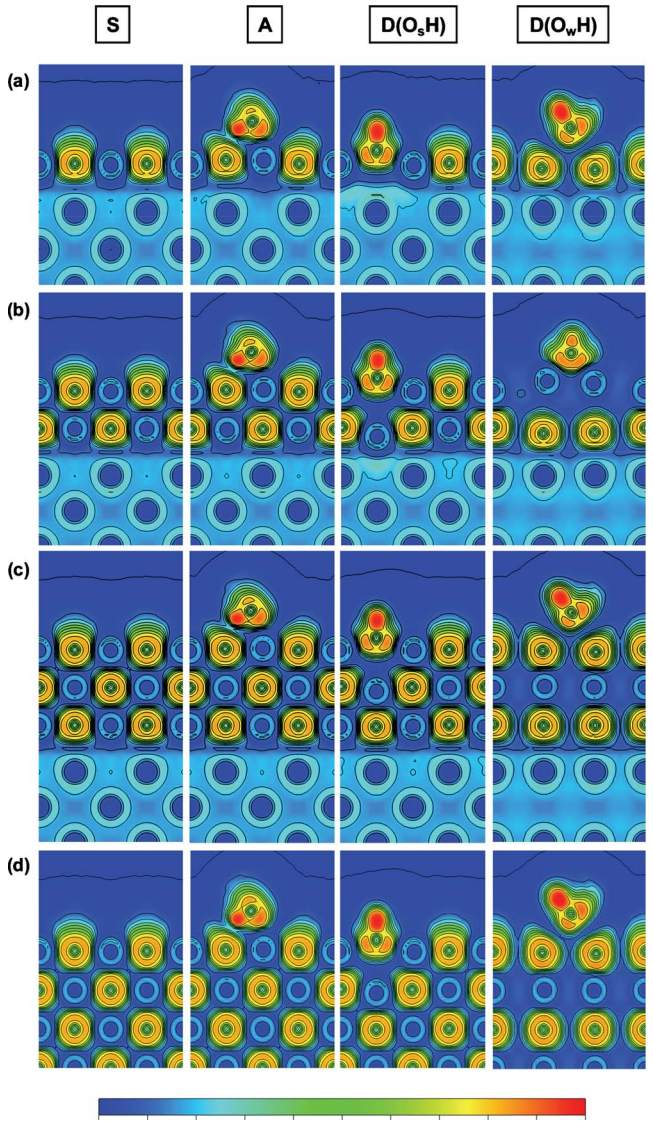


FIG. 3. (Color online) Side views of ELF maps before water adsorption (**S**), at a nondissociative adsorption state (**A**), and at a dissociative adsorption state (**D**) for (a)–(c) MgO(1, 2, and 3 ML)/Ag(100) and (d) MgO(100). $O_wH$ and $O_sH$ in the **D** state represent two hydroxyl ions produced by water dissociation. The former is directly produced by water dissociation and the latter is produced by $H^+$ bonding with a surface oxygen atom. The ELF map for the **D**($O_wH$) on the 2-ML film looks different due to the adsorption orientation of $O_wH$ species on the MgO film surface resulting from the rock salt structure of MgO, i.e., alternative $Mg^{2+}$-$O^{2-}$ ordering in the surface plane occurs depending on film thickness (see Fig. 2). H atoms of the adsorbed $O_wH$ are directed toward surface oxygen (see Fig. 1), which results in the difference in the orientation of $O_wH$ on the 2-ML MgO film surface of 90° compared to other surfaces with respect to an underlying metal substrate. However, there is no apparent difference in the electronic distribution, as well as in the adsorption structure, of adsorbates on the oxide surfaces with different thicknesses. Color and contour grid for the probability of finding the electron varies from 0 (blue) to 1 (red).

Charging of an adsorbate is considered crucial for controlling such adsorption properties as structure and energy. Recent experimental and theoretical studies reveal that the Au adsorbate,[29–32] whether a single atom or clusters, and molecular adsorbates, such as $O_2$ (Ref. 33) and $NO_2$,[34–36] can be charged on a thin oxide film surface. This interesting phenomenon has been explained by the charge transfer from the metal substrate or from the oxide-metal interface, which can be achieved by both the high electron affinity (EA) of an adsorbate and the work-function reduction in the metal substrate due to the existence of thin oxide film. Hellman *et al.* reported that the extent of adsorbate charging depends on film thickness.[36,37] We performed a Bader population analysis for adsorbates before and after water dissociation on MgO/Ag(100) to examine the adsorbate charging effect (Table III). The charge variation in individual adsorbates does not show strong dependence on film thickness for water dissociation ($\Delta Q < 0.1e$). The deviation from the formal charge of each adsorbate also is only within $0.12e$. This implies that there is no significant correlation between chemical activity and the charging effect depending on film thickness. In the present study, among dissociation products $H^+$ and $OH^-$ ($O_wH$), only $H^+$ is expected to have a large EA. However, the resulting proton forms a hydroxyl ion ($O_sH$) by bonding with a surface oxygen atom (Fig. 3). Therefore, no chemical species with large EA are formed during water dissociation on the MgO film surfaces supported by an Ag substrate. This is why the charge effect is not crucial for water dissociation on the metal-supported oxide film surface. In addition, the electron population in the Ag layer changes by no more than $0.15e$.

TABLE III. Bader populations (in $e$) of adsorbates for water dissociation on MgO($n$ ML)/Ag(100) ($n$=1, 2, and 3) and MgO(100) surfaces. $O_wH$ and $O_sH$ denote two hydroxyl ions produced by water dissociation, where the $H^+$ of dissociation products forms hydroxyl ions ($O_sH$) bonding with surface oxygen anions (see text).

| | 1 ML | 2 ML | 3 ML | Bulk |
|---|---|---|---|---|
| $H_2O$ | −0.08 | −0.07 | −0.07 | −0.07 |
| $O_wH$ | −0.87 | −0.88 | −0.88 | −0.88 |
| $H^+(O_sH)$ | +0.56(−0.93) | +0.63(−0.91) | +0.56(−0.91) | +0.57(−0.91) |

The DOS plots for the surface (adsorbate-oxide interaction) and interface (oxide-metal interaction) regions of the MgO films are shown in Figs. 4 and 5, respectively. In the DOS plots, the distribution of electronic states for the 1-ML MgO film is noticeably different from those for the 2-ML and 3-ML films. Since there is no ionic interaction between Mg and O in the $z$ axis at the 1-ML-thick MgO film, the oxygen of the MgO layer strongly hybridizes with the Ag substrate.[38] This phenomenon is also closely related to the stronger rumpling in the surface MgO layer of 1-ML film compared with the films of different thicknesses (Table II).

Figure 4 shows the change in electronic structures of adsorbates and the surface MgO layer for water dissociation. In Fig. 4(a), the peak positions of $O_wH$ are almost identical regardless of MgO thickness. However, the peak positions of $O_sH$ approach Fermi level as film thickness decreases, corresponding with the change in the surface electronic state distribution [**D** in Fig. 4(b)]. Therefore, the above-mentioned

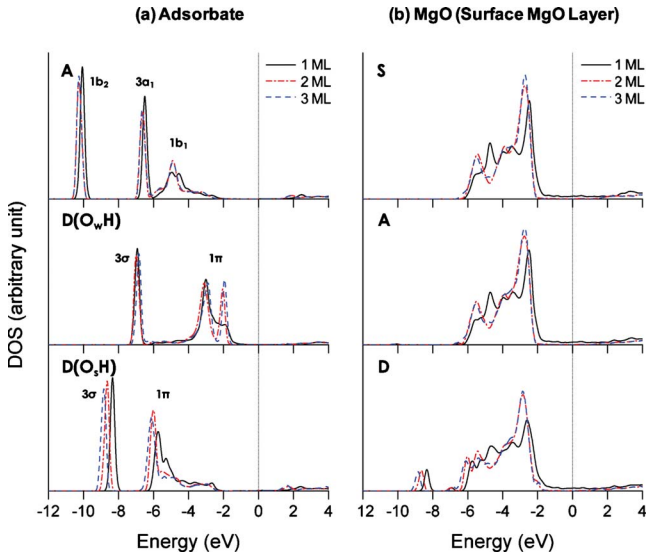


FIG. 4. (Color online) Local density of states of (a) adsorbates water molecule (**A**) and two hydroxyl ions [**D**($O_wH$) and **D**($O_sH$)] and (b) MgO (one surface layer) for MgO($n$ ML)/Ag(100) ($n$=1, 2, and 3) surfaces before water adsorption (**S**), at a nondissociative adsorption state (**A**), and at a dissociative adsorption state (**D**). The Fermi level is set at 0 eV.

difference in the peak position changes in $O_wH$ and $O_sH$ can be interpreted as evidence of the different kinds of interactions with the MgO film—electrostatic and covalent, respectively—shown in Fig. 3. While the $1\pi$ resonant state of $O_wH$ splits sharply into two peaks on the 2-ML and 3-ML MgO film surfaces, the peak broadening of the $O_wH$ $1\pi$ state for the 1-ML MgO film is observed at around 2 eV, indicating the effective interaction between $O_wH$ and the MgO surface layer at the 1-ML thickness. Similarly, the $1\pi$ state of $O_sH$ on the 1-ML MgO film surface also shows a relatively broad peak shape compared with thicker films. Although the difference in O-H distances between $O_wH$ and $O_sH$ is less than 1 Å on the all oxide film surfaces (Table I), their DOS plots show a different feature for the 1-ML MgO film than those for the 2-ML and 3-ML MgO films. This indicates that the two types of hydroxyls, $O_wH$ and $O_sH$, are more strongly influenced by the underlying metal substrate at the 1-ML MgO film than at the thicker films because the 1-ML MgO film interacts with both adsorbates and a metal substrate at the same time. In Fig. 4(b), the DOS features of the surface MgO layer do not show a significant change before (**S**) and after nondissociative adsorption (**A**) of the water molecule. However, in dissociative adsorption (**D**), the new electronic state of the surface MgO layer appears near −9 eV, due to the formation of $O_sH$ species and corresponding to the $3\sigma$ state of $O_sH$ in Fig. 4(a).

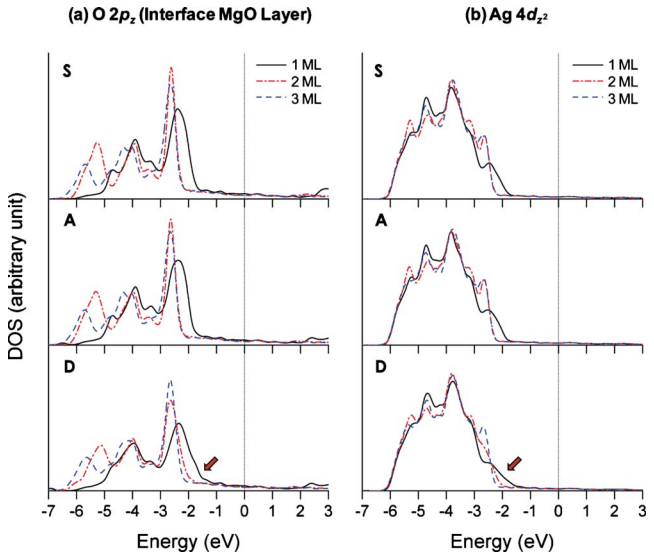


FIG. 5. (Color online) PDOS of the $z$ component of (c) Ag $4d$ and (d) O $2p$ states for MgO($n$ ML)/Ag(100) ($n$=1, 2, and 3) before water adsorption (**S**), at a nondissociative adsorption state (**A**), and at a dissociative adsorption state (**D**). PDOS are plotted for the oxide-metal interface region (MgO 1 layer+Ag 2 layers). The Fermi level is set at 0 eV.

Figures 5(a) and 5(b) show the projected DOS (PDOS) plots for the interface region between MgO film and Ag substrate during water dissociation with respect to the $z$ component of O $2p$ and Ag $4d$, respectively. The DOS feature for the individual MgO thickness at the interface is maintained before (**S**) and after nondissociative adsorption (**A**) of the water molecule. However, after water dissociation (**D**) for the 1-ML and 2-ML MgO films, the tails of the DOS plots broaden into the higher energy region (arrow in Fig. 5), which implies that the interaction between electronic states at the oxide-metal interface has increased. This agrees exactly with the previously demonstrated relationship between chemical activity and thickness changes, and demonstrates that the increased strength of covalent bonds between the oxide layer and the metal substrate at the oxide-metal interface plays an important role in enhancing chemical activity on the surface, although the covalent interaction between them is not as strong as ionic interaction within oxide layers. Therefore, the strong distortion of the interface structure is a consequence of the increased oxide-metal interaction strength at the interface as film thickness decreases (Table II and Fig. 2).

In summary, our computational results clearly show that catalytic activity on defect-free terrace sites of ultrathin MgO film surfaces can be enhanced compared with that achieved on their bulk counterpart. This strongly supports recent experimental results for water dissociation on a 1-ML MgO film.[9,10] The chemical activity of a metal-supported ultrathin oxide film can be controlled by film thickness without significant charge transfer from the substrate. This is closely correlated with both the geometric and the electronic natures of the oxide-metal interface because (1) the large interface distance allows severe geometric distortion caused by water dissociation and (2) the strong hybridization of the interface electronic states stabilizes the highly distorted oxide film.

Our results reveal that the film thickness and the adhesion between oxide and metal substrates are key factors in controlling the heterogeneous catalytic activity of an ultrathin oxide film supported by a metal substrate. That control can be achieved by manufacturing a thin oxide film with a well-defined thickness[14,15] and by the careful choice of a metal substrate. In addition, our results suggest that an ultrathin

oxide film supported by a metal substrate can be used to control catalytic reactions, even though the adsorbate is not activated or stabilized via the charge-transfer mechanism.[29,34] We believe that our findings can further understand the catalytic activity of ultrathin oxide films for water dissociation and provide an impetus for investigating thin oxide films for a wider range of applications.

This work was financially supported in part by a Grant-in-Aid for Scientific Research on Priority Areas "Electron Transport through a Linked Molecule in Nano-scale" and a Grant-in-Aid for Scientific Research(S) "Single Molecule Spectroscopy using Probe Microscope" from the Ministry of Education, Culture, Sports, Science, and Technology (MEXT), Japan, and in part by the Global COE Program (Chemistry Innovation through Cooperation of Science and Engineering), MEXT, Japan. We are grateful for the computational resources of the RIKEN Integrated Cluster of Clusters (RICC) supercomputer system. J.J. kindly acknowledges T. Iiitaka, Y. Morikawa, and S. Yanagisawa for fruitful discussion about computation and the International Program Associate (IPA) of RIKEN for financial support.

*Authors to whom correspondence should be addressed.
†FAX: +81-48-462-4663; ykim@riken.jp
‡maki@k.u-tokyo.ac.jp

[1] P. A. Thiel and T. E. Madey, Surf. Sci. Rep. **7**, 211 (1987).
[2] M. A. Henderson, Surf. Sci. Rep. **46**, 1 (2002).
[3] L. Giordano, J. Goniakowski, and J. Suzanne, Phys. Rev. Lett. **81**, 1271 (1998).
[4] F. Finocchi and J. Goniakowski, Phys. Rev. B **64**, 125426 (2001).
[5] Y. D. Kim, J. Stultz, and D. W. Goodman, J. Phys. Chem. B **106**, 1515 (2002).
[6] Y. Yu, Q. Guo, S. Liu, E. Wang, and P. J. Møller, Phys. Rev. B **68**, 115414 (2003).
[7] L. Savio, E. Celasco, L. Vattuone, and M. Rocca, J. Chem. Phys. **119**, 12053 (2003).
[8] L. Savio, E. Celasco, L. Vattuone, and M. Rocca, J. Phys. Chem. B **108**, 7771 (2004).
[9] S. Altieri, L. H. Tjeng, and G. A. Sawatzky, Phys. Rev. B **61**, 16948 (2000).
[10] S. Altieri, S. F. Contri, and S. Valeri, Phys. Rev. B **76**, 205413 (2007).
[11] A. M. Ferrari, C. Roetti, and C. Pisani, Phys. Chem. Chem. Phys. **9**, 2350 (2007).
[12] H.-J. Freund and G. Pacchioni, Chem. Soc. Rev. **37**, 2224 (2008).
[13] M. S. Chen and D. W. Goodman, J. Phys.: Condens. Matter **20**, 264013 (2008).
[14] H.-J. Shin, J. Jung, K. Motobayashi, S. Yanagisawa, Y. Morikawa, Y. Kim, and M. Kawai, Nature Mater. **9**, 442 (2010).
[15] S. Schintke, S. Messerli, M. Pivetta, F. Patthey, L. Libioulle, M. Stengel, A. De Vita, and W.-D. Schneider, Phys. Rev. Lett. **87**, 276801 (2001).
[16] H.-J. Freund, Surf. Sci. **601**, 1438 (2007).
[17] G. Kresse and J. Hafner, Phys. Rev. B **47**, 558 (1993).
[18] G. Kresse and J. Furthmüller, Phys. Rev. B **54**, 11169 (1996).
[19] J. P. Perdew and Y. Wang, Phys. Rev. B **45**, 13244 (1992).
[20] J. P. Perdew, J. A. Chevary, S. H. Vosko, K. A. Jackson, M. R. Pederson, D. J. Singh, and C. Fiolhais, Phys. Rev. B **46**, 6671 (1992).
[21] G. Kresse and D. Joubert, Phys. Rev. B **59**, 1758 (1999).
[22] S. Prada, U. Martinez, and G. Pacchioni, Phys. Rev. B **78**, 235423 (2008).
[23] J. A. Rodriguez, P. Liu, Y. Takahashi, K. Nakamura, F. Viñes, and F. Illas, J. Am. Chem. Soc. **131**, 8595 (2009).
[24] E. Sanville, S. D. Kenny, R. Smith, and G. Henkelman, J. Comput. Chem. **28**, 899 (2007).
[25] G. Henkelman, B. P. Uberuaga, and H. Jónsson, J. Chem. Phys. **113**, 9901 (2000).
[26] J. Carrasco, F. Illas, and N. Lopez, Phys. Rev. Lett. **100**, 016101 (2008).
[27] N. Lopez and S. Valeri, Phys. Rev. B **70**, 125428 (2004).
[28] G. Pacchioni, Surf. Sci. **520**, 3 (2002).
[29] G. Pacchioni, L. Giordano, and M. Baistrocchi, Phys. Rev. Lett. **94**, 226104 (2005).
[30] D. Ricci, A. Bongiorno, G. Pacchioni, and U. Landman, Phys. Rev. Lett. **97**, 036106 (2006).
[31] M. Sterrer, T. Risse, U. M. Pozzoni, L. Giordano, M. Heyde, H.-P. Rust, G. Pacchioni, and H.-J. Freund, Phys. Rev. Lett. **98**, 096107 (2007).
[32] V. Simic-Milosevic, M. Heyde, N. Nilius, T. König, H.-P. Rust, M. Sterrer, T. Risse, H.-J. Freund, L. Giordano, and G. Pacchioni, J. Am. Chem. Soc. **130**, 7814 (2008).
[33] A. Hellman, S. Klacar, and H. Grönbeck, J. Am. Chem. Soc. **131**, 16636 (2009).
[34] H. Grönbeck, J. Phys. Chem. B **110**, 11977 (2006).
[35] D. E. Starr, C. Weis, S. Yamamoto, A. Nilsson, and H. Bluhm, J. Phys. Chem. C **113**, 7355 (2009).
[36] A. Hellman and H. Grönbeck, Phys. Rev. Lett. **100**, 116801 (2008).
[37] P. Frondelius, A. Hellman, K. Honkala, H. Häkkinen, and H. Grönbeck, Phys. Rev. B **78**, 085426 (2008).
[38] J. Goniakowski and C. Noguera, Phys. Rev. B **79**, 155433 (2009).